Prediction of Core Electron Reactivity and High Oxidation States in Radium under High Pressure

Yihong Bai, a. Zhen Liu, a. Ling-Jun He, Fernando Ortega, Rafeed Khleif, Yuanzheng Chen, Liu, Ling-Jun He, Alaong Yan, a. Maosheng Miao^c, and Miao Rai, a. Wanzheng Chen, Alaong Yan, a. Maosheng Miao Rai, a. Wanzheng Chen, Alaong Yan, a. Wanzheng Miao Rai, a. Wanzheng Chen, Alaong Yan, a. Wanzheng Miao Rai, a. Wanzheng Chen, Alaong Yan, a. Wanzheng Chen, and Yan, a. Wanzheng Chen, and Yan, and Y

^aDepartment of Physics, Beijing Normal University, Beijing 100875, China

^bBeijing Computational Science Research Center, Beijing 100193, China

^cDepartment of Chemistry and Biochemistry, California State University Northridge, California 91330, United States

^dSchool of Physical Science and Technology, Southwest Jiaotong University, Chengdu 610031, China

[§]Y.B.

and Z.L. contributed equally to this work.

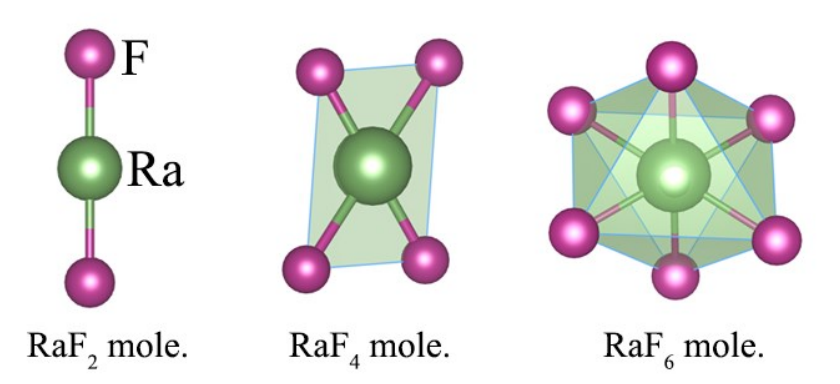
ABSTRACT: Recent first-principles calculations and crystal structure predictions revealed a striking phenomenon that the 5p core electrons of Cs can be activated and form covalent bonds with F under high pressure, causing the formation of unconventional CsF_n (n>1) compounds in which Cs can be oxidized up to +5 state. Despite many efforts, CsF_n remains the only example that the core electrons of a main group element become reactive. Here, we conduct an extensive crystal structure and stability prediction on Ra–F compounds under high pressure, which successfully identifies a series of stable compounds with high F stoichiometry (RaF_n, n = 3–8). By various electronic structure and bonding feature analyses, we demonstrate that the 6p core electrons of Ra are activated in most of these compounds and involved in forming covalent bonds with neighboring F atoms. Many novel phenomena emerge in RaF_n compounds whence the core electrons are activated, including oxidation states as high as +8, covalent Ra-F bonds, high-pressure molecular crystals, mixed-valence in RaF₃ and RaF₄ compounds, high coordination numbers, all of which point to a striking fact that Ra become a very different element under high pressure and exhibit very rich chemistry.

KEYWORDS: Radium polyfluoride, core electron chemistry, high oxidation states, first-principles calculation, crystal structure prediction.

Table of Contents (TOC)

Coordination No. of Ra increases with adding pressure

Promotes inner-shell 6p electrons of Ra to bond with F



INTRODUCTION

The oxidation state of elements in compounds is a key concept in chemistry and condensed-matter physics. 1-3 A general doctrine of chemistry is that the oxidation state of an element is determined by the number of its valence electrons. Many elements such as alkali metals assume one typical oxidation state while many others may have several different states under ambient pressure. Finding a new oxidation state of an element greatly extends the scope of chemistry and often opens a route to many new materials.^{3–5} Furthermore, achieving high oxidation state is an attractive goal in chemistry because the corresponding compounds could intrinsically be used as strong oxidants that can compel new types of chemical reactions. High oxidation states have been found in many species such as AuF₆, IF₇, [XeF₈]²⁻ and [WF₈]²⁻.^{2,6} Very recently, an unprecedented +8 oxidation state of Ir and I atoms is predicted in pressuredriven stable IrF8 and IF8 compounds. 7,8 Besides Ir, another record of the highest oxidation state of metals in stable compounds under ambient condition is +7 as found in Re(VII)F₇. Among all the species, high oxidation states in noble gases are particularly interesting because these elements have closed shell configurations and are very chemically inert. But once their closed shell electrons are activated by strong oxidants, as experimentally accomplished for the first time by Bartlett et al. who used PtF₆ to oxidize Xe and form Xe⁺[PtF₆]⁻, ¹⁰ there are more electrons available to achieve higher oxidation states.

To go one step further, it is an attractive conception to achieve higher oxidation state by activating the core electrons of main group elements other than noble gases. This turns out to be exceedingly difficult, and no attempt under ambient condition has led to a successful result. 11,12 Recently, with the use of first-principles calculations, we predicted that the inner-shell 5p electrons of Cs were activated under high pressure and form thermodynamically stable CsF_n (n=2-6) compounds, in which Cs atoms are oxidized beyond +1 valence state. 13-15 This breaks the doctrine that the oxidation states originate only from the outermost valance electrons based on the shell model.¹⁶ Moreover, high pressure might also cause the elements with semi-core 5d electrons to participate in forming bonds. For example, Hg atom could assume +4 oxidation state by forming HgF4 compound, 17 In contrast, the highest oxidation state of s-block elements currently reported is +5 in CsF₅ compound under high pressure, ¹³ although there are 9 electrons in 5s, 5p and 6s orbital of Cs atom in total. It is generally true that higher F composition in a compound correspond to high oxidation state. The previous studies show that Ba core electrons are much harder to be activated comparing with the core electrons of Cs.¹⁸ In order to activate more electrons to participate in forming bonds at high-pressure, we need to look for an alkali or alkaline metal whose first and second ionization potentials are comparable or even lower than that of Cs.

Radium (Ra) was discovered in 1898 by Pierre and Marie Curie, ¹⁹ and later was found almost ubiquitous in soils,

water, geologic materials, plants, and foods at low concentrations.²⁰ Owing to its widely application in radiation therapy,^{21–23} Ra chemistry has been thoroughly explored since its discovery.^{24–28} However, in all of its compounds, Ra is always in +2 oxidation state, in accordance to the fact that it has two valence electrons in its 7s orbital. Ra is constantly being produced by the radioactive decay of Uranium (U) and Thorium (Th) in Earth's crust and mantle.²⁹ Therefore, the study of its high-pressure chemistry can also help to understand the decay of U and Th in Earth's interior that is believed the most important thermos-source of the Earth.

In this work, aiming at exploring the potential high oxidation states of Ra, we conduct an extensive structure search based on first-principles calculations for F-rich RaF_n compounds with the compositions of n = 2-8 under high pressure (0–300 GPa). Our calculations show that Ra and F can form many stable compounds under pressure, including not only RaF₂ in which Ra is in the typical +2 oxidation state, but also higher F-composition compounds RaF_n (n=3 – 8), in which Ra assume higher oxidation states due to the activation of inner-shell electrons. Such unusual chemical behavior leads to substantial changes of the chemical properties of Ra and the structures of the corresponding Ra–F compounds. Remarkably, many Ra-F compounds contain molecular species under pressure, for example RaF6 consists of RaF₆ molecules in which Ra atom exhibits +6 oxidation state, exceeding the highest +5 state reported in sblock elements. In addition, RaF₈ is stable above 240 GPa, which is the most F-rich stoichiometry compound of s-block metal fluorides. Correspondingly, the coordination number of Ra reaches an unprecedented value of 12.

COMPUTATIONAL DETAILS

The structure searches of Ra-F compounds were carried out based on a global minimum search of the free energy landscape with respect to structural variations by combining particle swarm optimization (PSO) algorithm with firstprinciples calculations.^{30,31} We searched the structures for RaF_n (n=2-8) compounds at 0, 10, 100, 200 and 300 GPa, respectively. By evaluating the total energy of these structures, 60% of them with lowest enthalpies, together with 40% newly generated structures, are used to produce the structures of next generation by the structure operators of PSO. Applications of the method in numerous previous works show high accuracy and efficiency. 13,17,32-34 The geometry relaxations in the structure search and the formation enthalpies and electronic properties for the identified stable structures were calculated using density functional theory (DFT) as implemented in Vienna Ab initio Simulation Package (VASP) code. 35 The calculations were performed using a generalized gradient approximation (GGA)³⁶ within the framework of Perdew-Burke-Ernzerhof exchange-correlation functional.³⁷ The electronion interaction is described by the projector augmented wave³⁸ method with $6s^26p^67s^2$ and $2s^22p^5$ as valence electrons for Ra and F atoms, respectively. We adopted a

kinetic energy cutoff of 1400 eV for wave-function expansion and a k-point mesh of $2\pi \times 0.03$ Å⁻¹ or less for Brillouin zone integration. The structures (including lattice parameters and atomic positions) were fully optimized until the residual forces were converged within 0.02 eV/Å. The dynamical stability of predicted structures was determined by phonon calculations using the finite displacement approach³⁹ as implemented in the Phonopy code. ⁴⁰ Bader's Quantum Theory of Atoms in Molecules (QTAIM) analysis is employed for charge transfer analysis. ⁴¹ The Integrated Crystal Hamilton Population (ICOHP) was calculated using the Stuttgart version of the tight-binding LMTOs, atomic sphere approximation (TB–LMTO–ASA) programme. ⁴²

RESULTS AND DISCUSSION

The stability of Ra–F compounds. The stability of RaF_n compounds is examined by calculating the formation enthalpies defined as following:

$$h_!(\text{RaF}_") = \frac{\#(\%\&'_!))\#(\%\&'"_!)\frac{(!\$")\&('")}{"*+}}{"*+}$$
(1)

in which h_1 is the formation enthalpy per atom. We choose RaF₂ (Fm3m, same crystal form as calcium fluoride⁴³) as a reactant instead of Ra, because of the substantial stability of RaF2 throughout the studied pressure range. The relative thermodynamic stabilities of Ra-F compounds can be assessed by convex hulls (Fig. 1a). The compounds locate on these lines are stable against decomposition.⁴⁴ The pressure ranges of the stable composition are presented in Fig. 1b. The results show that besides RaF₂, RaF₄ can become stable at ambient pressure. However, the oxidation state of Ra in this compound is still +2, because it is a mixture of chain-like RaF₂ and F₂ molecule. Under high pressure, other Ra-F compounds with different stoichiometry (RaF_n, n =3, 5–8) might become stable. RaF₃ becomes stable at pressures of 48 GPa and remains stable up to 255 GPa. As the pressure further increases, the more Frich stoichiometry structures RaF5, RaF6, RaF7 and RaF₈ become stable at pressures of 78 GPa, 111 GPa, 180 GPa, and 240 GPa, respectively. It should be noted that some stable Ra-F compounds undergo a series of structural phase transitions with varying pressure (Fig. 1b). All the predicted stable compounds are found to be dynamically stable in view of the absence of imaginary phonon modes in the whole Brillouin zone (Figure S1).

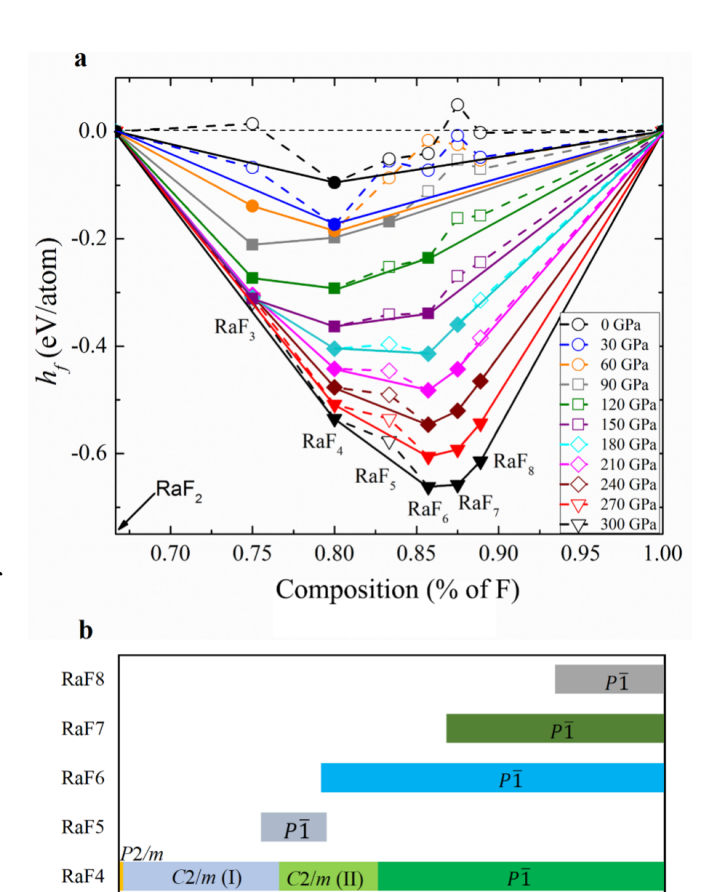


Figure 1. Convex hull and stability of RaF_n compounds under pressure. (a) The enthalpies of formation (eV/atom) from 0 to 300 GPa with steps of 30 GPa. The solid lines show the convex hull and the dash lines connect data points. (b) Predicted stable pressure range for RaF_n compounds.

150

Pressure (GPa)

200

250

300

100

50

Crystal structures. Selected structures for various compositions at their stable pressures are shown in Fig. 2, and the explicit structural information can be found in Table S1. RaF₃ adopts a structure with C2/c symmetry in the pressure range from 48 to 219 GPa (Fig. 2a). The Ra-F distances in RaF₃ at 90 GPa are in the range of 2.389–2.402 Å, shorter than that of RaF₂ (2.759 Å) at ambient pressure.⁴⁵ At higher pressure, RaF₃ undergoes a first-order transition to a structure with C2/m symmetry, which exhibits a distinctive crystal structure that consists of two types of Ra atoms and F atoms. Ra¹ forms square-planar RaF₄ molecular units that is similar to the square-planar structures observed in XeF₄, HgF₄ and AuF₄. ^{6,17,46} Ra² and neighboring F atoms present in the structure as non-bonded ions. calculations and bonding analysis also reveal that Ra¹ is in +4 oxidation state whereas Ra2 behaves as Ra2+ ions. Therefore, the C2/m RaF3 could be more accurately formulated as [Ra⁴⁺F₄]Ra²⁺(F⁻)₂. In the same fashion, the C2/c RaF₃ at lower pressure could be formulated as Ra³⁺F₃. In addition, the nearest F–F distance of 1.971 Å in C2/m

RaF3

0

RaF₃ (240 GPa) is significantly larger than the F–F bond length of 1.404 Å in F₂ molecule.⁴⁷ The disappearance of F₂ molecular feature in F rich compounds strongly indicates the involvement of inner-shell electrons in forming Ra–F bonds.

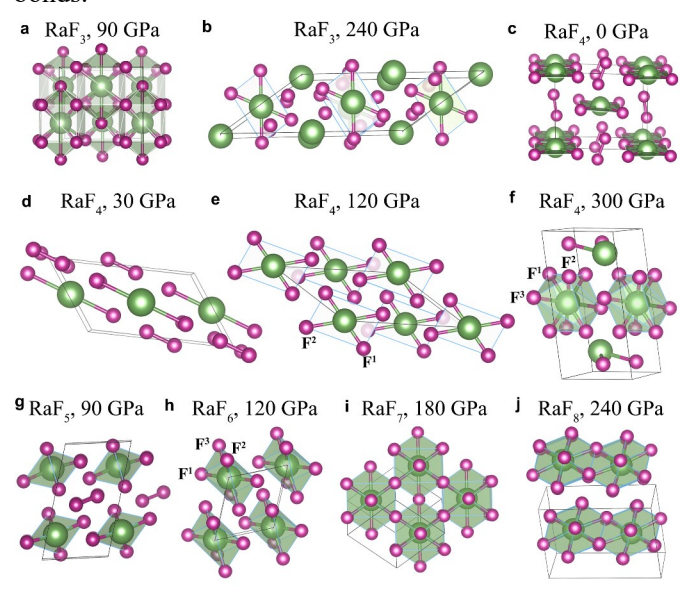


Figure 2. Crystal structures of stable RaF_n compounds. (a) C2/c RaF₃ at 90 GPa. (b) C2/m RaF₃ at 240 GPa. (c) P2/m RaF₄ at 0 GPa. (d) C2/m(I) RaF₄ at 30 GPa. (e) C2/m(I) RaF₄ at 120 GPa. (f) P'1 RaF₄ at 300 GPa. (g) P'1 RaF₅ at 90 GPa. (h) P'1 RaF₆ at 120 GPa. (i) P'1 RaF₇ at 180 GPa. (j) P'1 RaF₈ at 240 GPa. the green and purple spheres demote Ra and F atoms, respectively.

RaF₄ undergoes phase transitions from P2/m to C2/m(I) at 2 GPa (Fig. 2d), to C2/m (II) at 88 GPa (Fig. 2e), then to P1 at 142 GPa (Fig. 2f), respectively. Under lower pressure, P2/mRaF₄ contains edge sharing squareplanar RaF₄ ribbons and F₂ molecules. Moreover, C2/m (I) RaF4 contains F2 and linear RaF2 molecules that is isostructural to XeF₂⁴⁸. The Ra-F distance (2.518 Å at 30 GPa) in RaF₂ molecules is larger than the Cs–F bond length $(2.358 \text{ Å at } 20 \text{ GPa}) \text{ in CsF}_2$. Both P2/m and $C2/m(I) \text{ RaF}_4$ could be more accurately formulated as $[Ra^{2+}(F)_2]F_2$. At 120 GPa RaF₄ transforms into a C2/m (II) symmetry structure and is composed of multiple equivalent RaF4 planar molecules, which are similar to those in C2/mRaF₃. The major difference between them is that the molecules in RaF4 are almost square-planar, whereas those in RaF3 are largely distorted from perfect squares. While counting the oxidation state, the chemical formula of C2/m(II) RaF₄ becomes Ra⁴⁺F₄. Under higher pressure, RaF4 with P1 symmetry consists of two different units of RaF₈ and RaF₂ molecule. The RaF₈ unit is an 8-fold polyhedron, containing three types of Ra-F bond length (Ra-F¹, 1.880 Å; Ra-F², 1.885 Å; Ra-F³, 2.212 Å). The nearest F-F distance is 1.958 Å, much larger than the covalent F-F bond length of 1.440 Å, indicating that RaF₄ with P1 symmetry is a typical molecular crystal. The charge calculations (see below) also reveal that Ra is mixedvalent in P_1^{\dagger} RaF₄ which should be formulated as $[Ra^{6+}F_6]Ra^{2+}(F^-)_2$.

For more F-rich compounds RaF_n (n=5-8), all the identified structures with lowest enthalpy adopt P'1 symmetry. RaF₅ contains two RaF₄ tetrahedrons and a F₂ molecule (Fig. 2g) and it can be denoted as [Ra⁴⁺F₄]₂F₂. It has a very narrow stable pressure range from 78 to 113 GPa. As shown in Fig. 2h, RaF₆ is stable in a structure consisting of deformed octahedron molecules. At 120 GPa, six Ra-F bonds show three different lengths of 1.964, 2.030, and 2.040 Å. In addition, the nearest F–F distance between two RaF₆ units is 1.984 Å, much larger than the covalent F–F bond length of 1.440 Å, showing that RaF₆ is a molecular crystal. Therefore, its chemical formula is Ra⁶⁺F₆. RaF₇ stabilizes into a structure consisting of F edge- and vertexsharing RaF₁₂ polyhedra (Fig. 2i). Analogously, RaF₈ is also constructed as F edge-sharing RaF₁₂ polyhedra (Fig. 2j). The Ra-F distances in these polyhedra are in the range of 1.919–2.140 Å. More accurate analysis of the bonding characteristics will be discussed later. Ra atoms in both compounds show only one valence.

Electronic structures and the nature of Ra-F bonds. To investigate the electronic structures of RaF_n (n = 2-8), we calculated the projected density of states (PDOS) by projecting electron wavefunctions onto the atomic orbitals. The PDOS of RaF₄ with P2/m symmetry (0 GPa, Fig. 3a) and C2/m (I) symmetry (30 GPa, Fig. S2b) shows small overlap between Ra 6p and F 2p states. This is because these structures are composed of RaF₂ ribbon/molecule and F₂ molecule. Under high pressure, overlaps between Ra 6p and F 2p states near the Fermi level become more significant, suggesting charge transfers from Ra 6p to F 2p orbital in these RaF_n compounds (Fig. 3 and S2a-e). As the result of charge transfer, large Ra 6p components present above the Fermi level and its amount increases with increasing F composition.

Furthermore, by analyzing the COHP⁴⁹, we will show that once being activated, Ra 6p electrons participate in forming chemical bonds with neighboring F atoms. Different to PDOS, COHP can be negative/positive which reveal the bonding/antibonding nature of the states. Among the selected Ra-F, Ra-Ra, and F-F pairs, COHP of Ra-F bond is the most negative one. The calculated COHP (Fig. 3d, f, h) shows that the overlaps between 6p states of Ra and 2p states of its nearest neighboring F atom are around -10.5 eV, -13.0 eV, and -10.0 eV for C2/m (II) RaF₄, P'1RaF₄, and P1 RaF₆, respectively. Moreover, the integrated COHPs (ICOHPs) up to the Fermi level can be used to measure the bong strength. The calculated ICOHPs are -2.640 and -0.524 eV/pair for Ra-F1 and Ra-F2 bonds in C2/m (II) RaF₄ (120 GPa) and are -2.697, -2.584, and -0.818 eV/pair for three non-equivalent bonds in P1 RaF₄ (300 GPa), respectively. The ICOHPs of Ra-F pair are found to be -2.695, -2.125 and -1.995 eV/pair for P'1 RaF₆ (120 GPa). Comparing to the -0.335 eV/pair in RaF₂ (a typical ionic crystal) under 30 GPa, the bonds in these

Ra-F compounds are highly covalent. We also notice that the ICOHP of F-F pair in P1 RaF₆ is as low as -0.039 eV/pair, which confirms F atoms do not form bonds and the compound is formed by crystalizing RaF₆ molecules. The

Ra-F ICOHP in RaF₅, RaF₇ and RaF₈ show an overall trend of enhancement with the increase of coordination number (Table S2). This is caused by the increasing number of activated inner-shell Ra 6*p* electrons, which enhance the strength of interactions in Ra–F bonds.

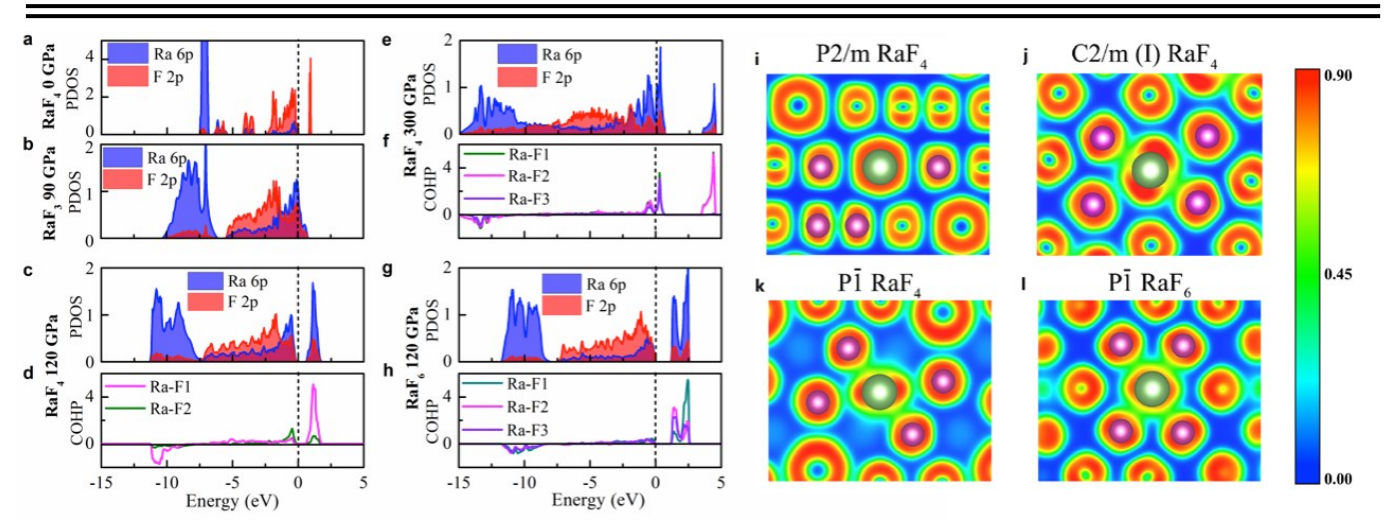


Figure 3. Electronic structures and the nature of Ra–F bonds. (a) PDOS (state/eV/atom) for RaF4 at 0 GPa. (b) PDOS for RaF3 at 90 GPa. (c) PDOS and (d) COHP for RaF4 at 120 GPa. (e) PDOS and (f) COHP for RaF4 at 300 GPa. (g) PDOS and (h) COHP for RaF6 at 120 GPa. ELFs of (i) RaF4 at 0 GPa [(0 0 1) plane]. (j) RaF4 at 120 GPa [(0 1 0) plane]. (k) RaF4 at 300 GPa [(0 1 0) plane]. (l) RaF6 at 120 GPa [Ra–F¹–F² plane].

These bonding features of Ra–F compounds are also supported by the electron localization function (ELF) analysis. ^{50–52} Larger ELF values usually correspond to inner shell or lone pair electrons and covalent bonds, whereas the ionic bonds correspond to small ELF values. As shown in Fig. 3i, the *P2/m* RaF4 is quite ionic in nature. However, large ELF values occur between nearest neighboring Ra and F atoms, indicating a covalent bonding character. More information about the bonding analysis can be found in Table S2 and Fig. S3.

Ra oxidation states are beyond +2 state based on above analysis because Ra exhibits multiple covalent bonds with neighboring F atoms in RaF_n (n = 3-8). To further examine this view, we calculate the charges using Bader's quantum theory of atoms in molecules (QTAIM)⁴¹ analysis. As shown in Fig. 4a, the charges of Ra steadily increase with higher F composition (selected at 120 GPa and 250 GPa), and are beyond +2 state in RaF_n for compounds with n>2. We note that the Bader charges are usually notably smaller than the formal oxidation numbers, even for typical ionic crystals such as RaF₂ (1.68 at 30 GPa), and are more so for covalent or molecular compounds. As an independent validation, the wavefunction-based Mulliken and Löwdin charges of Ra–F (Fig. S4) are comparable to the evolutions of the density-derived Bader charge results in Fig. 4a.

Fig. 4a reveals very different charge transfer trends at the two calculated pressures. At 120 GPa, the Bader charge increases with increasing F composition while n<6, except that RaF₆ shows a similar Bader charge as RaF₄, which is consistent with the fact that Ra in RaF₅ ([Ra⁴⁺F₄]₂F₂) is actually in +4 state. The Bader charges in RaF₇ and RaF₈ under 120 GPa are lower than that of RaF₆. However, both

two compounds are not stable at this pressure. Bader charges at 250 GPa show a striking feature, namely there are two very different values in RaF₃ and RaF₄, corroborating with the aforementioned mixed valence of Ra in these two compounds.

If average Bader charges are used to represent RaF₃ and RaF₄, the Bader charges increase quite linearly with the increasing F composition (Fig. 4a), strongly suggesting the same increasement of the nominal oxidation state of Ra in these compounds. Thus, despite the actual charge values calculated by Bader's QTAIM method, the nominal oxidation state of Ra can be assigned. For example, Ra in RaF₆ is in +6 state, although the calculated Bader charges are 3.1 and 3.3 under 120 and 250 GPa. Furthermore, the Bader charge increases monotonically for n>5, indicating a continuously growing oxidation number. Therefore, it is reasonable to assign nominal oxidation states of +7 and +8 to Ra atoms in RaF₇ and RaF₈.

In addition, the coordination numbers of Ra also increase with higher F composition, which also corroborate the high oxidation states, because the activation of more core electrons from Ra cause the formation of more Ra-F bonds and prevent the formation of F-F bonds. It is worth mentioning that the coordination number of Ra in RaF₈ is 12, which is one of the highest among all *s*-metal compounds as Ba²⁺ in Ba(SbF₆)₂·5XeF₂.⁴⁸

The reactivity of the core electrons is driven by the change and reordering of the orbital energies of s/p-block electron of Ra and the p-block electrons of F. To reveal this point, we calculated the atomic orbital energy levels of F 2p, Cs 5p, Ba 5p, and Ra 6p, under high pressure using a He matrix model (Figure 4b). Although the energies of all

atomic orbitals increase with pressure, Cs 5p and Ba 5p orbitals increase more significantly than F 2p, surpassing the later at ~16 GPa and ~224 GPa, respectively, which agrees well with the previous atomic orbital calculations^{13,18} and with the stable pressure regions of Cs-F compounds as predicted in the previous studies. Similarly, Ra 6p becomes higher in energy than F 2p at ~92 GPa, which is consistent with the structure and stability predictions in this work. In addition, the Ra 6p bands significantly broaden as the pressure increases, which further elevates the energy level of 6p orbitals, causing more Ra 6p electrons being transferred to F atoms. Both points are important for the gradual stabilization of F-rich compounds (RaF₆ \rightarrow RaF₇ \rightarrow RaF₈) with increasing pressure.

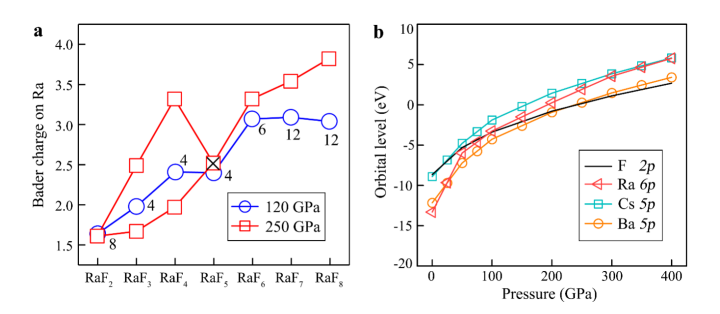


Figure 4. (a) Calculated Bader charge for Ra in RaF_n compounds at 120 GPa (blue line) and 250 GPa (red line). The number to the right of the symbol indicates the coordination number of Ra in each Ra–F compound. (b) Energies of F 2p, Ra 6p, Cs 5p, and Ba 5p orbitals as a function of the external pressure. Pressure effect is modeled by putting elements in a face-centered cubic supercell $(3\times3\times3)$ He matrix, in which one He atom is replaced by the atom being examined.⁵³

Recent studies have illustrated that Cs can react with F and form unusual F-rich compounds under high pressure, exhibiting the chemical characteristics like *p*-block elements. Ba—F compounds also show large portion of 5*p* components close to the Fermi level, although they do not exhibit *p*-block compound properties such as forming molecular crystals. Our results clearly show a new example that an *s*-metal can behave like a *p*-block element under pressure, due to the activation of its core electrons. Remarkably, the highest nominal oxidation number can be as high as +8, surpass the previously reported +5 in CsF₅, which sets a new record of oxidation number of alkali and alkaline metals.

CONCLUSIONS

To conclude, using swarm-intelligence based computational structure search, we explored the enthalpy landscape of RaF_n (n = 2-8) under high-pressure condition. A series of stable RaF_n compounds have been predicted, in which Ra shows a formal oxidation state beyond +2 based on the analysis of PDOS, ELF and QTAIM charges. In most of these compounds, the inner-shell Ra 6p electrons are

reactive and are prone to form strong covalent bonds with F atoms. Strikingly, RaF6 exhibits a molecular crystal feature with +6 oxidation state of Ra. The coordination number of Ra in RaF8 reaches 12, which is among the highest in all s-block metal fluorides. This coordination number has been observed before in a complex hexafluorantimoates Ba(SbF6)2·5XeF2.⁴⁸

ASSOCIATED CONTENT

Supporting Information

The Supporting Information is available free of charge at https://pubs.acs.org. Phonon spectra, structural parameters, projected density of states, ICOHP of selected RaF_n compounds.

AUTHOR INFORMATION

*Corresponding Authors

*E-mail: <u>yuanhui.sun@csun.edu</u> *E-mail: <u>yandd@bnu.edu.cn</u> *E-mail: <u>mmiao@csun.edu</u>

ORCID

Yuanhui Sun: 0000-0003-2981-1133 Maosheng Miao: 0000-0001-9486-1204

Notes

The authors declare no competing financial interest.

ACKNOWLEDGMENT

Y.S. and M.M. acknowledge the support of NSF under the grant No. DMR-1848141, and computational resources provided by XSEDE (TG-DMR130005). M.M. also acknowledges the support of ACS PRF 50249-UNI6 and the support of California State University Research, Scholarship and Creative Activity (RSCA) awards. D.Y. acknowledge the support of National Natural Science Foundation of China for the grant under Nos 21873015. Z.L. also acknowledge National Natural Science Foundation of China support for the funding under Nos 12004045. L.H. is supported by the China Postdoctoral Science Foundation under grants No. 2021M690326.

REFERENCES

- (1) Karen, P.; McArdle, P.; Takats, J. Toward a Comprehensive Definition of Oxidation State (IUPAC Technical Report). *Pure and Applied Chemistry* **2014**, *86* (6), 1017–1081. https://doi.org/10.1515/pac-2013-0505.
- (2) Riedel, S.; Kaupp, M. The Highest Oxidation States of the Transition Metal Elements. *Coordination Chemistry Reviews* **2009**, *253* (5), 606–624. https://doi.org/10.1016/j.ccr.2008.07.014.
- (3) Wang, G.; Zhou, M.; Goettel, J. T.; Schrobilgen, G.

- J.; Su, J.; Li, J.; Schlöder, T.; Riedel, S. Identification of an Iridium-Containing Compound with a Formal Oxidation State of IX. *Nature* **2014**, *514*, 475. https://doi.org/10.1038/nature13795
- (4) Windorff, C. J.; Chen, G. P.; Cross, J. N.; Evans, W. J.; Furche, F.; Gaunt, A. J.; Janicke, M. T.; Kozimor, S. A.; Scott, B. L. Identification of the Formal +2 Oxidation State of Plutonium: Synthesis and Characterization of Pu^{II}[C₅H₃(SiMe₃)₂]₃}⁻. *J. Am. Chem. Soc.* **2017**, *139* (11), 3970–3973. https://doi.org/10.1021/jacs.7b00706.
- (5) Zhang, Q.; Hu, S.-X.; Qu, H.; Su, J.; Wang, G.; Lu, J.-B.; Chen, M.; Zhou, M.; Li, J. Pentavalent Lanthanide Compounds: Formation and Characterization of Praseodymium(V) Oxides.

 Angewandte Chemie International Edition 2016, 55 (24), 6896–6900. https://doi.org/10.1002/anie.201602196.
- (6) Lin, J.; Zhang, S.; Guan, W.; Yang, G.; Ma, Y. Gold with +4 and +6 Oxidation States in AuF₄ and AuF₆.

 Journal of the American Chemical Society 2018, 140 (30), 9545–9550. https://doi.org/10.1021/jacs.8b04563.
- (7) Lin, J.; Zhao, Z.; Liu, C.; Zhang, J.; Du, X.; Yang, G.; Ma, Y. IrF₈ Molecular Crystal under High Pressure. *J. Am. Chem. Soc.* **2019**, *141* (13), 5409–5414. https://doi.org/10.1021/jacs.9b00069.
- (8) Luo, D.; Lv, J.; Peng, F.; Wang, Y.; Yang, G.; Rahm, M.; Ma, Y. A Hypervalent and Cubically Coordinated Molecular Phase of IF₈ Predicted at High Pressure. *Chem Sci* 2019, 10 (8), 2543–2550. https://doi.org/10.1039/c8sc04635b.
- (9) Vogt, T.; Fitch, A. N.; Cockcroft, J. K. Crystal and Molecular Structures of Rhenium Heptafluoride. *Science* 1994, 263 (5151), 1265–1267. https://doi.org/10.1126/science.263.5151.1265. (24)
- (10) Bartlett, N. Proc. Chem. Soc. *Proc. R. Chem. Soc.* **1962**, *1962*, 218.
- (11) Moock, K.; Seppelt, K. Indications of Cesium in a Higher Oxidation State. *Angewandte Chemie International Edition in English* **1989**, 28 (12), 1676–1678. https://doi.org/10.1002/anie.198916761.
- (12) Jehoulet, C.; Bard, A. J. On the Electrochemical Oxidation of Cs⊕ and Other Alkali-Metal Ions in Liquid Sulfur Dioxide and Acetonitrile. *Angewandte Chemie International Edition in English* **1991**, *30* (7), 836–838. https://doi.org/10.1002/anie.199108361.
- (13) Miao, M. S. Caesium in High Oxidation States and as a *p*-Block Element. *Nat Chem* **2013**, *5* (10), 846–852. https://doi.org/10.1038/nchem.1754.
- (14) Zhu, Q.; Oganov, A. R.; Zeng, Q. Formation of Stoichiometric CsF_n Compounds. *Scientific Reports* **2015**, *5* (1), 7875. https://doi.org/10.1038/srep07875.
- (15) Sonnenberg, K.; Mann, L.; Redeker, F. A.; Schmidt, B.; Riedel, S. Polyhalogen and Polyinterhalogen Anions from Fluorine to Iodine. *Angewandte Chemie International Edition* **2020**, *59* (14), 5464–

- 5493. https://doi.org/10.1002/anie.201903197.
- (16) van der Put, P. J. The Chemical Bond. In *The Inorganic Chemistry of Materials: How to Make Things out of Elements*; van der Put, P. J., Ed.; Springer US: Boston, MA, 1998; pp 31–86.
- (17) Botana, J.; Wang, X.; Hou, C.; Yan, D.; Lin, H.; Ma, Y.; Miao, M. Mercury under Pressure Acts as a Transition Metal: Calculated from First Principles. *Angewandte Chemie International Edition* **2015**, *54* (32), 9280–9283. https://doi.org/10.1002/anie.201503870.
- (18) Luo, D.; Wang, Y.; Yang, G.; Ma, Y. Barium in High Oxidation States in Pressure-Stabilized Barium Fluorides. *J Phys Chem C* **2018**, *122* (23), 12448–12453. https://doi.org/10.1021/acs.jpcc.8b03459.
- (19) Curie, P.; Curie, M.; B??mont, G.; Becquerel, H. Sur une nouvelle substance fortement radio-active: contenue dans la pechblende. *Comptes rendus hebdomadaires des séances de l'Académie des sciences.* **1898**, No. 26.
- (20) Gad, S. C. Radium. In *Encyclopedia of Toxicology* (*Third Edition*); Wexler, P., Ed.; Academic Press: Oxford, 2014; pp 44–45.
- (21) Vdovenko, V. M.; Dubasov, Y. V. Analytical Chemistry of Radium; Analiticheskaya Khimiya Radiya; Izdatel'stvo Nauka, Leningrad, 1973.
- (22) Kjellgren, O.; Ragnhult, I. Armamentarium for Radium Treatment of Carcinoma of the Uterine Cervix. *Acta Radiologica: Therapy, Physics, Biology* **1963**,*1* (1), 1–22. https://doi.org/10.3109/02841866309135060.
 - Sciaroni, G. H. Radium in the Treatment of Sarcoma and Carcinoma. *International Journal of Orthodontia* **1918**, 4 (12), 655–658. https://doi.org/10.1016/S1072-3471(18)90122-7.
 - Matyskin, A. V.; Ebin, B.; Tyumentsev, M.; Allard, S.; Skarnemark, G.; Ramebäck, H.; Ekberg, C. Disassembly of Old Radium Sources and Conversion of Radium Sulfate into Radium Carbonate for Subsequent Dissolution in Acid. *J Radioanal Nucl Chem* **2016**, *310* (2), 589–595. https://doi.org/10.1007/s10967-016-4927-x.
- (25) Matyskin, A. V.; Ylmen, R.; Lagerkvist, P.; Ramebäck, H.; Ekberg, C. Crystal Structure of Radium Sulfate: An X-Ray Powder Diffraction and Density Functional Theory Study. *Journal of Solid State Chemistry* 2017, 253, 15–20. https://doi.org/10.1016/j.jssc.2017.05.024.
- (26) Matyskin, A. V.; Hansson, N. L.; Brown, P. L.; Ekberg, C. Barium and Radium Complexation with Ethylenediaminetetraacetic Acid in Aqueous Alkaline Sodium Chloride Media. *J Solution Chem* 2017, 46 (11), 1951–1969. https://doi.org/10.1007/s10953-017-0679-7.
- (27) Matyskin, A. V.; Brown, P. L.; Ekberg, C. Weak Barium and Radium Hydrolysis Using an Ion Exchange Method and Its Uncertainty Assessment. *The Journal of Chemical Thermodynamics* **2019**,

(23)

- *128*, 362–371. https://doi.org/10.1016/j.jct.2018.08.037.
- (28) Brown, P. L.; Ekberg, C.; Matyskin, A. V. On the Solubility of Radium and Other Alkaline Earth Sulfate and Carbonate Phases at Elevated Temperature. *Geochimica et Cosmochimica Acta* **2019**, 255, 88–104. https://doi.org/10.1016/j.gca.2019.04.009.
- (29) Radioactivity: The Earth's Heat. https://www.radioactivity.eu.com/site/pages/Earth_Heat.htm (accessed 2020-12-03).
- (30) Kennedy, J.; Eberhart, R. Particle Swarm Optimization. In *Proceedings of ICNN'95 International Conference on Neural Networks*; 1995; Vol. 4, pp 1942–1948 vol.4. https://doi.org/10.1109/ICNN.1995.488968.
- (31) Eberhart; Yuhui Shi. Particle Swarm Optimization: Developments, Applications and Resources. In *Proceedings of the 2001 Congress on Evolutionary Computation (IEEE Cat. No.01TH8546)*; 2001; Vol. 1, pp 81–86 vol. 1. https://doi.org/10.1109/CEC.2001.934374.
- (32) Peng, F.; Miao, M.; Wang, H.; Li, Q.; Ma, Y. Predicted Lithium–Boron Compounds under High Pressure. *J. Am. Chem. Soc.* **2012**, *134* (45), 18599–18605. https://doi.org/10.1021/ja308490a.
- (33) Sun, Y.; Li, Y.; Li, T.; Biswas, K.; Patanè, A.; Zhang, L. New Polymorphs of 2D Indium Selenide with Enhanced Electronic Properties. *Advanced Functional Materials* **2020**, *30* (31), 2001920. https://doi.org/10.1002/adfm.202001920.
- (34) Li, Q.; Zhou, D.; Zheng, W.; Ma, Y.; Chen, C. Global Structural Optimization of Tungsten Borides. *Phys. Rev. Lett.* **2013**, *110* (13), 136403. https://doi.org/10.1103/PhysRevLett.110.136403.
- (35) Kresse, G.; Furthmüller, J. Efficient Iterative Schemes for Ab Initio Total-Energy Calculations Using a Plane-Wave Basis Set. *Phys. Rev. B* **1996**, *54*, 11169–11186.
- Perdew, J. P.; Chevary, J. A.; Vosko, S. H.; Jackson, (36)K. A.; Pederson, M. R.; Singh, D. J.; Fiolhais, C. Molecules, Solids, and Surfaces: **Applications** of the Generalized Gradient Approximation for Exchange and Correlation. Phys. Rev. 1992. (11),6671-6687. https://doi.org/10.1103/PhysRevB.46.6671.
- (37) Perdew, J. P.; Burke, K.; Ernzerhof, M. Generalized Gradient Approximation Made Simple. *Phys. Rev. Lett.* **1996**, 77, 3865–3868.
- (38) Kresse, G.; Joubert, D. From Ultrasoft Pseudopotentials to the Projector Augmented-Wave Method. *Phys. Rev. B* **1999**, *59*, 1758–1775.
- (39) Parlinski, K.; Li, Z. Q.; Kawazoe, Y. First-Principles Determination of the Soft Mode in Cubic ZrO₂. *Phys. Rev. Lett.* **1997**, 78 (21), 4063–4066. https://doi.org/10.1103/PhysRevLett.78.4063.
- (40) Togo, A.; Oba, F.; Tanaka, I. First-Principles Calculations of the Ferroelastic Transition between

- Rutile-Type and CaCl₂-Type SiO₂ at High Pressures. *Phys. Rev. B* **2008**, 78 (13), 134106. https://doi.org/10.1103/PhysRevB.78.134106.
- (41) Bader, R. F. W. Atoms in Molecules. *Acc. Chem. Res.* **1985**, *18* (1), 9–15. https://doi.org/10.1021/ar00109a003.
- (42) The STUTTGART TB-LMTO-ASA program. https://www2.fkf.mpg.de/andersen/LMTODOC/L MTODOC.html (accessed 2022-06-09).
- (43) Ropp, R. C. Chapter 2 Group 17 (H, F, Cl, Br, I) Alkaline Earth Compounds. In *Encyclopedia of the Alkaline Earth Compounds*; Ropp, R. C., Ed.; Elsevier: Amsterdam, 2013; pp 25–104. https://doi.org/10.1016/B978-0-444-59550-8.00002-8.
- (44) Feng, J.; Hennig, R. G.; Ashcroft, N. W.; Hoffmann, R. Emergent Reduction of Electronic State Dimensionality in Dense Ordered Li-Be Alloys. *Nature* **2008**, *451* (7177), 445–448. https://doi.org/10.1038/nature06442.
- (45) Schulze, G. E. R. Die Kristallstruktur von Radiumfluorid. *Zeitschrift für Physikalische Chemie* **1936**, 32B (1), 430–432. https://doi.org/10.1515/zpch-1936-3236.
- (46) Ibers, J. A.; Hamilton, W. C. Xenon Tetrafluoride: Crystal Structure. *Science* **1963**, *139* (3550), 106–107. https://doi.org/10.1126/science.139.3550.106.
- Ivlev, S. I.; Karttunen, A. J.; Hoelzel, M.; Conrad, M.; Kraus, F. The Crystal Structures of α- and β-F2 Revisited. *Chemistry A European Journal* 2019, 25 (13), 3310–3317. https://doi.org/10.1002/chem.201805298.
- (48) Chernick, C. L.; Claassen, H. H.; Fields, P. R.; Hyman, H. H.; Malm, J. G.; Manning, W. M.; Matheson, M. S.; Quarterman, L. A.; Schreiner, F.; Selig, H. H.; Sheft, I.; Siegel, S.; Sloth, E. N.; Stein, L.; Studier, M. H.; Weeks, J. L.; Zirin, M. H. Fluorine Compounds of Xenon and Radon. *Science* 1962, 138 (3537), 136–138. https://doi.org/10.1126/science.138.3537.136.
- (49) Dronskowski, R.; Blöchl, P. E. Crystal Orbital Hamilton Populations (COHP): Energy-Resolved Visualization of Chemical Bonding in Solids Based on Density-Functional Calculations. *J. Phys. Chem.* **1993**, 97 (33), 8617–8624. https://doi.org/10.1021/j100135a014.
- (50) Burdett, J. K.; McCormick, T. A. Electron Localization in Molecules and Solids: The Meaning of ELF. *J. Phys. Chem. A* **1998**, *102* (31), 6366–6372. https://doi.org/10.1021/jp9820774.
- (51) Silvi, B.; Savin, A. Classification of Chemical Bonds Based on Topological Analysis of Electron Localization Functions. *Nature* **1994**, *371* (6499), 683–686. https://doi.org/10.1038/371683a0.
- 52) Savin, A.; Nesper, R.; Wengert, S.; Fässler, T. F. ELF: The Electron Localization Function. *Angewandte Chemie International Edition in English* **1997**, *36* (17), 1808–1832.

- https://doi.org/10.1002/anie.199718081.
- (53) Miao, M.-S.; Hoffmann, R. High Pressure Electrides: A Predictive Chemical and Physical Theory. *Acc. Chem. Res.* **2014**, 47 (4), 1311–1317. https://doi.org/10.1021/ar4002922.
- (54) Rogachev, A. Y.; Miao, M.-S.; Merino, G.; Hoffmann, R. Molecular CsF5 and CsF2+. *Angew Chem Int Ed Engl* **2015**, *54* (28), 8275–8278. https://doi.org/10.1002/anie.201500402.